Adhesion of mineral and soot aerosols can strongly affect their scattering and absorption properties

Michael I. Mishchenko[1,*] and Janna M. Dlugach[2]

[1]*NASA Goddard Institute for Space Studies, 2880 Broadway, New York, New York 10025, USA*

[2]*Main Astronomical Observatory of the National Academy of Sciences of Ukraine, 27 Zabolotny Street, 03680 Kyiv, Ukraine*

**Corresponding author: michael.i.mishchenko@nasa.gov*

Received December 13, 2011; revised December 23, 2011; accepted December 25, 2011; posted January 4, 2012 (Doc. ID 159918); published February 14, 2012

We use the numerically exact superposition T-matrix method to compute the optical cross sections and the Stokes scattering matrix for polydisperse mineral aerosols (modeled as homogeneous spheres) covered with a large number of much smaller soot particles. These results are compared with the Lorenz–Mie results for a uniform external mixture of mineral and soot aerosols. We show that the effect of soot particles adhering to large mineral particles can be to change the extinction and scattering cross sections and the asymmetry parameter quite substantially. The effect on the phase function and degree of linear polarization can be equally significant.

OCIS codes: 290.0290, 290.1090, 290.5825, 290.5850.

Mineral and soot particles are ubiquitous constituents of natural and artificial environments [1–5]. Both particle types can have quite complex morphologies [2–4], thereby making the calculation of their scattering and absorption properties highly nontrivial and necessitating the use of a combination of computer solvers of the macroscopic Maxwell equations with supplementary ranges of performance characteristics [6,7]. As if to aggravate the problem even further, the morphologically complex mineral and soot particles can stick to each other and form various types of compound aerosols. Whether the optical properties of a mixture of mineral and soot particles change upon aggregation depends on the strength of the electromagnetic interaction between the mineral and soot components, which can now be in direct physical contact instead of being widely separated. This interaction and the resulting optical effects are still insufficiently understood and poorly quantified, and so they constitute the main subject of this Letter.

Depending on the specific type of environment, one can expect a varying range of morphologies of the individual mineral and soot particles. However, the main focus of this Letter is not on the optical effects of individual-particle morphology (see [6,8–12]) but rather on the potential effects of small soot particles adhering to the surfaces of larger mineral hosts. It is therefore appropriate to constrain the scope of this study by choosing the simplest morphology of the individual mineral and soot aerosols in the form of homogeneous spheres. This choice also allows us to use the highly efficient and numerically exact superposition T-matrix method (STMM) [13,14].

Our model of a compound mineral–soot particle is illustrated by the inset in Fig. 1, wherein the surface of a relatively large mineral particle is covered by a number N_s of small soot particles. This model differs from those analyzed in [10] in that the soot particles are assumed to be compact, thereby corresponding to the stage in their aging when fluffy soot fractals have already collapsed into densely packed aggregates with fractal dimensions approaching 3 [4,15]. The ratio of the radius of the mineral host to that of the small soot particles is kept constant at $R/r \equiv 10$. Soot particles are placed on the surface of a large mineral host using a random-number generator and making sure that the particles do not overlap. The scattering and absorption characteristics of the compound aerosols are then averaged over the uniform orientation distribution of the resulting cluster as well as over a standard power law distribution $n(R) = \text{constant} \times R^{-3}$ [8] with an effective radius $R_{\text{eff}} = 1\ \mu$m, effective variance $v_{\text{eff}} = 0.05$, and host radii in the range $0.661\ \mu\text{m} \le R \le 1.439\ \mu$m. The resulting effective radius of the soot particles ($r_{\text{eff}} = 0.1\ \mu$m) is typical of the postcollapse stage [4,15]. The refractive index of the mineral hosts is $1.55 + i0.0003$, while that of the soot particles is $1.75 + i0.435$. The wavelength is fixed at $0.62832\ \mu$m. The averaging over cluster orientations is performed using the efficient semianalytical procedure afforded by the STMM [13]. The numerical size averaging is based on the Gauss–Legendre quadrature formula with 100 nodes. The size averaging has a dual purpose of (i) better representing polydisperse particle ensembles encountered in various applications and (ii) smoothing out artifacts in the form of sharp resonance features typical of monodisperse scatterers [8].

The solid curves in Fig. 1 visualize the elements of the normalized Stokes scattering matrix relating the Stokes parameters of the incident quasi-monochromatic light and those of the scattered light:

$$\begin{bmatrix} I^{\text{sca}} \\ Q^{\text{sca}} \\ U^{\text{sca}} \\ V^{\text{sca}} \end{bmatrix} \propto \begin{bmatrix} a_1(\Theta) & b_1(\Theta) & 0 & 0 \\ b_1(\Theta) & a_2(\Theta) & 0 & 0 \\ 0 & 0 & a_3(\Theta) & b_2(\Theta) \\ 0 & 0 & -b_2(\Theta) & a_4(\Theta) \end{bmatrix} \begin{bmatrix} I^{\text{inc}} \\ Q^{\text{inc}} \\ U^{\text{inc}} \\ V^{\text{inc}} \end{bmatrix}, \tag{1}$$

where $\Theta \in [0°, 180°]$ is the angle between the incidence and scattering directions; both sets of the Stokes parameters are defined with respect to the scattering plane

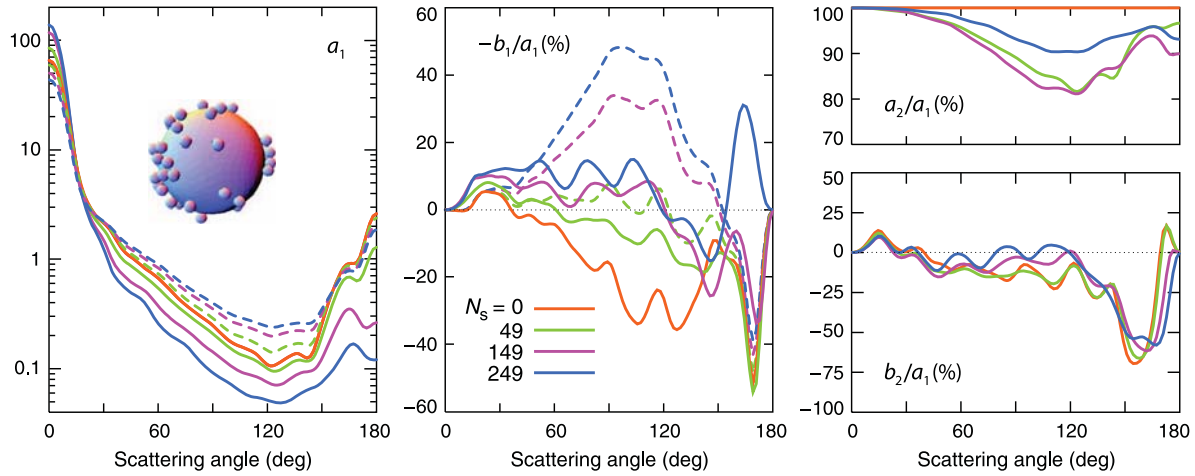

Fig. 1. Solid curves depict the elements of the size- and orientation-averaged Stokes scattering matrix for a large mineral particle covered randomly by N_s small soot particles. The inset illustrates the morphology of the compound aerosols and shows a mineral host covered with $N_s = 49$ soot particles. Dashed curves depict the Lorenz–Mie results for a composition-equivalent external mixture of mineral and soot aerosols.

[8]. The (1,1) element of the scattering matrix is the conventional phase function normalized according to

$$\frac{1}{2}\int_0^\pi d\Theta \sin\Theta a_1(\Theta) = 1. \quad (2)$$

The corresponding integral radiometric characteristics are listed in Table 1. These STMM results are paralleled by the results of Lorenz–Mie computations based on the assumption that each mineral host and the respective N_s soot particles are all widely separated and scatter light independently of each other.

The comparison of these two sets of results can be used to identify and quantify specific optical effects of aggregation. It is obvious that depending on N_s, these effects can be quite strong. At least some of them can be interpreted qualitatively.

First, increasing N_s always increases the extinction and absorption cross sections, but this increase is slower in the case of the compound aerosols because the large mineral hosts shade almost half of the soot particles and thus preclude them from interacting with the incident field. Second, increasing the number of strongly absorbing soot particles always results in a decrease of the single-scattering albedo. It is interesting, however, that this effect is virtually the same for compound aerosols and the uniform external mixture of mineral and soot aerosols. Third, the effects of increasing N_s on the scattering cross sections and asymmetry parameters of the compound aerosols and of the uniform external mixture are exactly opposite. The asymmetry parameter of the external mixture decreases with N_s because the asymmetry parameter of the Rayleigh-like soot particles is much smaller than that of the large mineral hosts. In the case of compound aerosols, increasing N_s causes the formation of a strongly absorbing coating around the weakly absorbing mineral core, especially when soot particles cover a significant fraction of the host's surface. The resulting phase function is increasingly controlled by the forward-scattering diffraction peak and the first external reflection, thereby becoming progressively anisotropic. This coating also suppresses the contribution of the host to the scattering cross section. Overall, Table 1 demonstrates that aggregation can result in a decrease of the optical cross sections by almost a factor of 2 as well as in significantly larger asymmetry parameters approaching 0.9.

The left-hand panel of Fig. 1 demonstrates potentially very strong effects of aggregation on the phase function. For example, the solid and dashed blue curves exhibit a factor of 4.5 differences at side scattering angles and 1 order of magnitude differences at backscattering angles. The middle panel of Fig. 1 is also indicative of potentially strong effects of aggregation on the degree of linear polarization for unpolarized incident light given by $P(\Theta) = -b_1(\Theta)/a_1(\Theta)$. In particular, the solid and dashed blue curves exhibit at backscattering angles a strong positive maximum and a deep negative minimum,

Table 1. Ensemble-Averaged Extinction, Scattering, and Absorption Cross Sections (in μm^2) per Compound Aerosol Particle, Single-Scattering Albedo ω, and Asymmetry Parameter g as Functions of the Number of Small Soot Particles Covering the Surface of a Large Mineral Host[a]

N_s	C_{ext}	C_{sca}	C_{abs}	ω	g	C'_{ext}	C'_{sca}	C'_{abs}	ω'	g'
0	6.314	6.265	0.049	0.9923	0.668	6.314	6.265	0.049	0.9923	0.668
49	6.925	5.678	1.247	0.820	0.730	8.279	6.924	1.355	0.836	0.635
149	7.832	5.161	2.671	0.659	0.819	12.291	8.268	4.023	0.673	0.585
249	8.485	5.086	3.399	0.599	0.876	16.302	9.611	6.691	0.590	0.549

[a]The primed characteristics correspond to the case of a uniform external mixture of widely separated, independently scattering mineral and soot aerosols

respectively, which almost mirror each other with respect to the horizontal $P(\Theta) = 0$ line.

The ratio $a_2(\Theta)/a_1(\Theta)$ is identically equal to unity for the external mixture of spherical mineral and soot particles but deviates from unity noticeably for compound aerosols, thereby signifying the nonsphericity of the latter (see the right-hand upper panel of Fig. 1). The change of this ratio with N_s is highly nonmonotonic. By the time N_s reaches the value 249, soot particles form a quasi-uniform coating around the mineral host, thereby making the compound particle quasi-spherical. This appears to explain the smaller deviation of the blue curve from 100% than those of the green and pink curves. Overall, the deviation of the ratio $a_2(\Theta)/a_1(\Theta)$ from unity appears to be too weak to make this ratio useful in optical particle characterization.

The ratio $b_2(\Theta)/a_1(\Theta)$ appears to be even less sensitive to the presence of soot particles. Indeed, the right-hand bottom panel of Fig. 1 as well as the respective Lorenz–Mie results for the external mixture of mineral and soot aerosols (not shown) show rather weak changes with increasing N_s.

In summary, our numerically exact STMM and Lorenz–Mie results demonstrate that the effect of small soot particles adhering to large mineral particles can be to change the optical cross sections and the asymmetry parameter quite substantially. The effect on the phase function and degree of linear polarization can be equally dramatic. There is no reason to expect that these conclusions will change significantly if one considers nonspherical rather than spherical mineral hosts, especially in the case of the integral radiometric characteristics.

These conclusions are fundamentally different from those drawn in [16] on the basis of similar computations but performed for large mineral hosts covered with much smaller mineral grains of the same chemical composition. There is no doubt that this difference is primarily caused by soot particles being much more absorbing than size-equivalent mineral grains.

We expect that our results will be important in analyses of laboratory and remote-sensing data as well as in assessments of radiative aerosol effects on climate (e.g., [17–19]). The quantitative significance of our findings may vary depending on the type of environment and the specific application. The strong dependence of the effects of aggregation on N_s obviously indicates the urgent need for accurate measurements of the state of aggregation of mineral and soot aerosols as well as of their relative number densities in various types of environment.

We thank Ping Yang and an anonymous referee for constructive reviews. This research was partly funded by the NASA Radiation Sciences Program managed by Hal Maring and by the NASA Remote Sensing Theory Program managed by Lucia Tsaoussi. We also acknowledge support from the National Academy of Sciences of Ukraine under the Main Astronomical Observatory GRAPE/GPU/GRID Computing Cluster Project.

References

1. E. J. Daivs and G. Schweiger, *The Airborne Microparticle* (Springer, 2002).
2. J. Li, J. R. Anderson, and P. R. Buseck, J. Geophys. Res. **108**, 4189 (2003).
3. E. A. Reid, J. S. Reid, M. M. Meier, M. R. Dunlap, S. S. Cliff, A. Broumas, K. Perry, and H. Maring, J. Geophys. Res. **108**, 8591 (2003).
4. R. Zhang, A. F. Khalizov, J. Pagels, D. Zhang, H. Xue, and P. H. McMurry, Proc. Natl. Acad. Sci. USA **105**, 10291 (2008).
5. P. Kukri, P. A. Baron, and K. Willeke, *Aerosol Measurement* (Wiley, 2011).
6. M. I. Mishchenko, J. W. Hovenier, and L. D. Travis, *Light Scattering by Nonspherical Particles* (Academic, 2000).
7. F. M. Kahnert, J. Quant. Spectrosc. Radiat. Transfer **79–80**, 775 (2003).
8. M. I. Mishchenko, L. D. Travis, and A. A. Lacis, *Scattering, Absorption, and Emission of Light by Small Particles* (Cambridge University, 2002), http://www.giss.nasa.gov/~crmim/books.html.
9. O. Dubovik, A. Sinyuk, T. Lapyonok, B. N. Holben, M. Mishchenko, P. Yang, T. F. Eck, H. Volten, O. Muñoz, B. Veihelmann, W. J. van der Zande, J.-F. Leon, M. Sorokin, and I. Slutsker, J. Geophys. Res. **111**, D11208 (2006).
10. L. Liu and M. I. Mishchenko, J. Quant. Spectrosc. Radiat. Transfer **106**, 262 (2007).
11. L. Liu, M. I. Mishchenko, and W. P. Arnott, J. Quant. Spectrosc. Radiat. Transfer **109**, 2656 (2008).
12. M. Kahnert and A. Devasthale, Atmos. Chem. Phys. **11**, 11745 (2011).
13. D. W. Mackowski and M. I. Mishchenko, J. Opt. Soc. Am. A **13**, 2266 (1996).
14. D. W. Mackowski and M. I. Mishchenko, J. Quant. Spectrosc. Radiat. Transfer **112**, 2182 (2011).
15. K. A. Lewis, W. P. Arnott, H. Moosmüller, R. K. Chakrabarty, C. M. Carrico, S. M. Kreidenweis, D. E. Day, W. C. Malm, A. Laskin, J. L. Jimenez, I. M. Ulbrich, J. A. Huffman, T. B. Onasch, A. Trimborn, L. Liu, and M. I. Mishchenko, Atmos. Chem. Phys. **9**, 8949 (2009).
16. M. I. Mishchenko, J. M. Dlugach, and D. W. Mackowski, Opt. Lett. **36**, 337 (2011).
17. T.-H. Lin, P. Yang, G.-R. Liu, and F. Tsai, Proc. SPIE **8177**, 81770L (2011).
18. J. Hansen, T. Bond, B. Cairns, H. Gaeggler, B. Liepert, T. Novakov, and B. Schichtel, Eos Trans. Amer. Geophys. Union **85**, 241 (2004).
19. S. E. Bauer, S. Menon, D. Koch, T. C. Bond, and K. Tsigaridis, Atmos. Chem. Phys. **10**, 7439 (2010).